ECS Journal of Solid State Science and Technology, **1** (5) Q91-Q95 (2012)
2162-8769/2012/1(5)/Q91/5/$28.00 © The Electrochemical Society

Study of Resistive Switching Characteristics on a Temperature-Sensitive FeO_x-Transition Layer in a $TiN/SiO_2/FeO_x/Fe$ Structure

Yao-Feng Chang,[a] Yu-Ting Tsai,[b,*] Geng-Wei Chang,[c] Yong-En Syu,[d] Ya-Hsiang Tai,[c] and Ting-Chang Chang[d,e,z]

[a]*Department of Electrical and Computer Engineering, The University of Texas at Austin, Texas 78758, USA*
[b]*Department of Electronics Engineering and Institute of Electronics, National Chiao Tung University, Hsinchu 300, Taiwan*
[c]*Department of Photonics & Institute of Electro-Optical Engineering, National Chiao Tung University, Hsinchu 300, Taiwan*
[d]*Department of Physics, National Sun Yat-set University, Kaohsiung 804, Taiwan*
[e]*Advanced Optoelectronics Technology Center, National Cheng Kung University, Tainan 701, Taiwan*

Thermal annealing effect and high temperature electrical measurement were studied on a temperature-sensitive FeO_x-transition layer of a $TiN/SiO_2/FeO_x/Fe$ structure, including bipolar switching behaviors, statistics of set and reset electrical characteristics, endurance and retention. Increase of the thermal budget on the structure shrinks both the operation voltage and variation as well as improving the device operation stability and power dissipation. Cross-sectional image, crystallinity and chemical composition analyzes of the FeO_x-transition layer were examined by transmission electron microscope, X-ray diffraction and X-ray photon-emission spectra depth profiles, respectively. In addition, for the temperature-sensitive FeO_x-containing structure, the resistive switching behaviors and characteristics were also investigated at room temperature and 85°C. These resistive switching behaviors indicate the possible resistive switching mechanism and electrical characteristics, providing a better understanding for the temperature-sensitive FeO_x-based memristors.
© 2012 The Electrochemical Society. [DOI: 10.1149/2.003205jss] All rights reserved.

Manuscript submitted May 8, 2012; revised manuscript received July 30, 2012. Published September 5, 2012.

Recently, resistance random access memory (RRAM), phase change memory and discrete nanocrystal memory attract extensive interest for being promising candidates of next generation nonvolatile memory devices due to their excellent advantages of high cell density array, high operation speed, low power consumption, low cost, and high retention.[1–5] For RRAM, several kinds of resistive switching mechanisms have been reported.[6–8] However, the exact switching mechanisms have not yet been clarified and are still under debate. For transition metal oxide systems, the resistive switching behaviors between high-resistance state (HRS) and low-resistance state (LRS) are strongly associated with the inevitable existence of nonstoichiometric chemical composition in the resistive switching materials.[9–12] Therefore, it is necessary to examine in detail the relationship between material's nonstoichiometric properties and its resistive switching characteristics, specifically the effect of temperature, which affects the chemical redox reaction severely. In our previous reports,[13,14] we proposed a method to fabricate a nonstoichiometric FeO_x layer by oxidizing a Fe-containing electrode spontaneously while depositing a plasma-enhanced TEOS (Tetraethyl Orthosilicate, PE-TEOS) oxide onto the Fe-containing electrode, i.e. a FeO_x-transition layer formed in a SiO_2/FeO_x/Fe-containing electrode structure. Interestingly, the nonstoichiomerty of such the FeO_x-containing structures is markedly sensitive to temperature,[15,16] causing changes in the physical phase crystallinity, and chemical composition as well as the further diffusion of Fe atoms from Fe-containing electrode into the SiO_2 layer. Therefore, in this study, we mainly focus on the resistive switching behaviors and their electrical characteristics in such temperature-sensitive structures by performing different thermal treatment conditions and testing the devices under high temperature environment. By detailed analyzes of the bottom-up electrical statistic characteristics and resistive switching behavior, we can get more understanding of the FeO_x-containing memristor and its possible resistive switching mechanism. These results can help us design and optimize the FeO_x-based memristor's performance for future nonvolatile memory applications.

Experimental

Fabrication of resistive switching device.— The FeO_x-containing memristors were prepared through the following processes, the details were shown in our previous reports.[13,14] After thermal oxidation of *p*-type (100) silicon wafers, a 50-nm-thick Pt layer and then a 50-nm-thick Fe layer were deposited as a bottom electrode by DC magnetron sputtering of Pt and Fe targets. A 50-nm-thick SiO_2 layer was deposited on the bottom electrode by a plasma enhanced chemical vapor deposition system with substrate temperature of 350°C and a working pressure of (TEOS (50 sccm) + O_2 (300 sccm)) gases at 500 mTorr. The top electrode, 50-nm-thick TiN, was sputtered and patterned in a square area with side length of 100 μm on the SiO_2 film. Finally, rapid thermal annealing (RTA) treatments at 600°C for different intervals of 30 sec (denoted as "RTA-30 sec sample"), and 60 sec (denoted as "RTA-60 sec sample"), and a furnace annealing (FA) treatment at 600°C for 30 min (denoted as FA-30 min sample) were performed in Argon ambient. For comparison, a control sample without the annealing treatment (denoted as "as-deposited sample") was also prepared under the same process.

Characterization analysis.— A Keithley 4200 semiconductor characterization system was used to measure the current-voltage (*I-V*) characteristics of the fabricated devices. In addition, Auger electron spectroscopy (AES) and transmission electron microscope (TEM) were carried out using a VG Microlab 350 and a Philips Tecnai-20 System, respectively. X-ray diffraction (XRD) was carried out using a PANalytical X'Pert Pro (MRD) with a monochromatized Cu Kα; λ = 0.154 nm. Furthermore, X-ray photoelectron spectroscopy (XPS) was also carried out using the Microlab 350 with a monochromatized Al Kα X-ray source (1486.6 eV; 300 W). In order to gain more insight during the resistance switching process, electric parameters of critical switching conditions were extracted for all the samples. The definition of the "Set Current/Reset Current (I_{set})/(I_{reset})" and "Set Voltage/Reset Voltage (V_{set})/(V_{reset})" are the values of the current and voltage detected at the beginning of the resistance switching from a HRS/LRS to a LRS/HRS, respectively. The "Set Power/Reset Power (P_{set})/(P_{reset})" is defined as the product of I_{set}/I_{reset} and V_{set}/V_{reset}.

Results and Discussion

Material examination and analysis.— Figure 1a and 1b show cross-sectional TEM image and energy dispersive X-ray (EDX) analyzes in the as-deposited $TiN/SiO_2/FeO_x/Fe/Pt$ structure. With the aid of local EDX analysis, one can study the chemical compositions of

*Electrochemical Society Student Member.
zE-mail: tcchang@mail.phys.nsysu.edu.tw

Downloaded on 2014-04-28 to IP 140.113.38.11 address. Redistribution subject to ECS terms of use (see ecsdl.org/site/terms_use) unless CC License in place (see abstract).

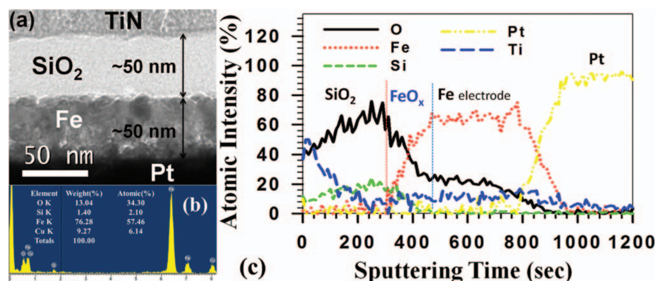

Figure 1. (a) Cross-sectional TEM of the TiN/SiO_2/FeO_x/Fe/Pt structure, (b) EDX analysis for FeO_x-transition layer. (c) AES depth profiles of O, Fe, Si, Pt and Ti on TiN/SiO_2/FeO_x/Fe/Pt structure.

specific interesting regions with high space resolution. The thickness of each layer can be confirmed by TEM analysis. It was further observed that there was a thin gray layer of about (or below) 5 nm in thickness between SiO_2 and the bottom Fe layer, associated with the FeO_x-transition region by EDX analysis. The FeO_x-transition region was due to the ease of oxidation of iron atoms under the PE-TEOS deposition conditions (TEOS and O_2 ambient under 350°C substrate temperature). Of note, the unexpected Cu and Si contaminations are regarded as being introduced from the TEM grid and the substrates in the process of ion-beam thinning, respectively. In order to get more detailed analysis about the FeO_x-transition layer in the device, AES depth profiles of O, Fe, Si, Pt and Ti in the TiN/SiO_2/FeO_x/Fe/Pt stacked layers were performed, as shown in the Fig. 1c. In Fig. 1c, a non-abrupt transition of both Fe and O elements from high to low atomic concentrations was distinctly observed. Fe and O overlapped in the same region, i.e. the transition region, showing the existence of non-stoichiometric iron oxides. Furthermore, the Si element was nearly undetectable in the bulk of the Fe electrode, indicating the absence of silicidation inside the Fe electrode. Of note, the oxygen penetrated into the Fe electrode would be detected by the AES, which is due to the single Fe electrode would be easier oxidized in the oxygen ambient compared to the alloy FePt electrode.[13,17]

The phase crystallinity and chemical composition of the FeO_x-transition layer due to different thermal treatment conditions were also examined by using XRD and XPS depth profiles, as shown in the Figs. 2 and 3. Figure 2 depicts XRD (θ-2θ) data of the as-deposited, RTA-30 sec, RTA-60 sec and FA-30 min samples for the SiO_2/FeO_x/Fe/Pt stacked structure. It is observed that there is a distinct enhancement of Pt (111) peak intensities and also the appearance of additional Fe_2O_3 (222), Fe_2O_3 (012), Fe_2O_3 (111) and FeO (111) peaks after the annealing treatments.[18] It indicates that crystallinity ordering of the FeO_x-transition layer has been formed and changed during the thermal annealing, resulting in the partial transformation of the metastable iron oxide (FeO) into the thermodynamically stable phases (Fe_2O_3).[15,16] Similarly, Fig. 3 shows the FeO_x chemical states by analyzing XPS depth profiles of Fe-*2p* on the as-deposited, RTA-60 sec and FA-30 min samples (The XPS results of RTA-30 sec sample are similar to the RTA-60 sec sample, therefore, its data are not shown here). Ar ions were used for sputter etching into the SiO_2 layer to collect the XPS data at various depths and the corresponding etching times of the spectra as shown in Fig. 3 are in series of 300, 330, 360, and 400 sec from bottom to top. Of note, besides the existence of the nonstoichiometric iron oxides, FeO (709.8 eV), Fe_2O_3 (711.4 eV), and Fe_3O_4 (710.4 eV),[13] are detected the corresponding binding energy in all the samples, higher Fe-O bond intensities as well as Fe-Fe (707.3 eV) bond intensities in the thermal-treated samples are clearly detected at shorter Ar sputter etching times as compared to the similar depth in the as-deposited sample. This observation related to a deeper diffusion of Fe atoms into SiO_2 layer under post-thermal treatment process and resulted in early collecting the Fe-related signals. Also, for all the samples, it is noted that detection of relatively higher binding intensities and areas of FeO_x phases (FeO, Fe_2O_3, and Fe_3O_4) compared to the Fe-Fe phase is obtained, which means that a higher intensity ratio of Fe-O bindings to Fe-Fe bindings was formed in the FeO_x-transition layer. The reason is that the diffusion of Fe atoms could ease formation the oxidation states of Fe-O bonds rather than remained Fe atoms during the post-thermal treatment or

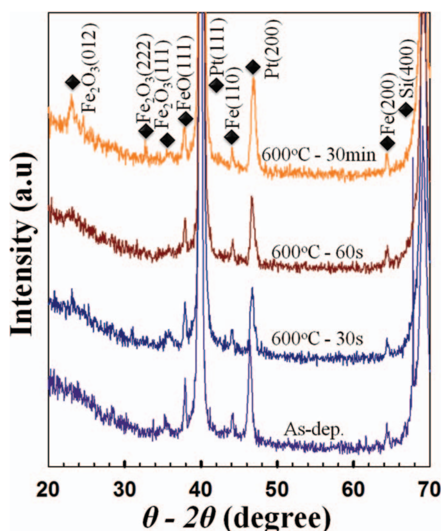

Figure 2. XRD θ-2θ scan results of the SiO_2/FeO_x/Fe/Pt structures without (as-deposited condition) and with a thermal treatment of RTA-30 sec, RTA-60 sec and FA-30 min at 600°C. Symbol (♦) indicates the diffraction peaks appeared for different samples and contributed from the crystallinity of Si, Pt, Fe and FeO_x phases.

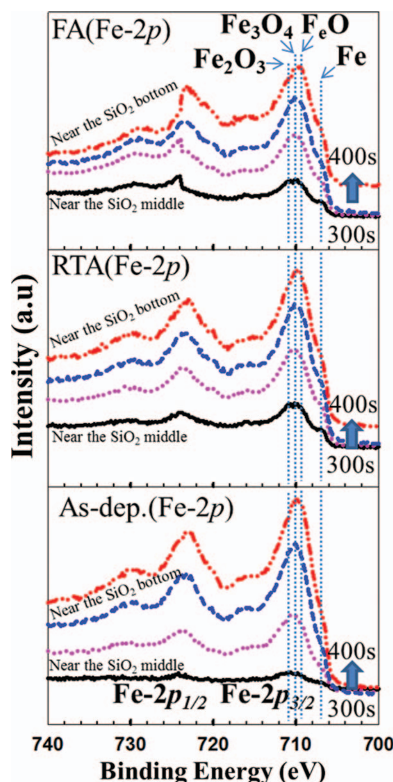

Figure 3. XPS depth profiles of Fe-*2p* on the SiO_2/FeO_x/Fe/Pt structures without (as-deposited condition) and with a thermal treatment of RTA-60 sec and FA-30 min at 600°C. The depth profiles are obtained by an Ar sputter etching in the SiO_2 layer, collecting the XPS data at various depths. The etching times of the spectra are from bottom to top 300, 330, 360, and 400 sec.

Downloaded on 2014-04-28 to IP 140.113.38.11 address. Redistribution subject to ECS terms of use (see ecsdl.org/site/terms_use) unless CC License in place (see abstract).

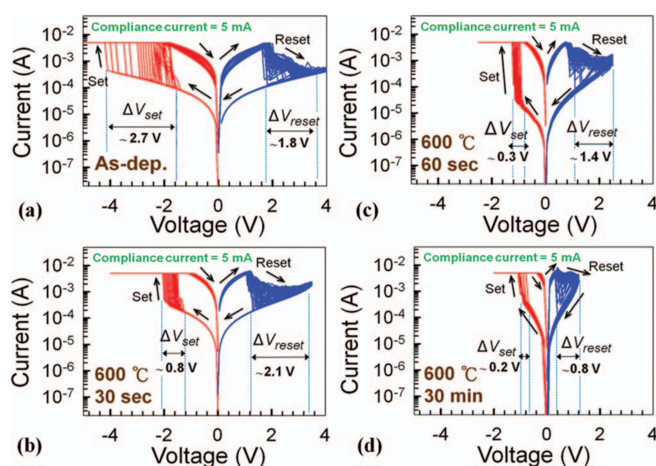

Figure 4. 50-cycle bipolar switching behaviors of the (a) as-deposited, (b) RTA-30 sec, (c) RTA-60 sec and (d) FA-30 min at 600°C thermal-treated samples. The arrows indicate the voltage sweeping directions and variations of set and reset voltage value.

PE-TEOS deposited processes. These XPS results are also consistent with the higher peak ratio between FeO_x and Fe in XRD results under post-thermal treatment process.

Resistance switching behavior in post-thermal treatment effect.— Figure 4 shows the *I-V* electrical characteristics of the as-deposited, RTA-30 sec, RTA-60 sec and FA-30 min samples for 50 cycles of repeating switching measurements. The driving voltage was biased on the bottom electrode while the top electrode was ground in 3 samples which always obtained consistent results, and also, the compliance current was limited to 5 mA to prevent the hard breakdown during sweeping voltage. Bipolar switching is observed for all the samples on sweeping the voltage from 0 V to positive values, the current begins to decrease gradually or dramatically at a reset voltage (V_{reset}) and finally reaches a HRS. On the other hand, the current increases suddenly at a set voltage (V_{set}) and returns to a LRS while sweeping the voltage to negative values. In addition, besides a reduction in operation voltages (V_{set} and V_{reset}), the variances of V_{set} (ΔV_{set}) and V_{reset} (ΔV_{reset}) were also improved as the annealing time increased. According to the proposed switching mechanism of iron oxides explained by a chemical redox reaction of FeO_x[16] between the Fe_3O_4 phase (with lower resistance[19]) and Fe_2O_3 phase (with higher resistance[20]), we suggest that the improved crystallinity of the FeO_x film, i.e. been already existed crystalline phases of Fe_2O_3 structure in the annealed sample, could cause the ease of such iron oxide phase transformation between Fe_3O_4 and Fe_2O_3 so as to reduce the operation voltages as well as their variations.[14] The other possible explanation for the improvement of these resistive switching characteristics is that: it may result from the severe Fe ions diffusion effect, which means that these diffused Fe ions in the SiO_2 may form an impurity band in the insulator then take an interaction with the metal electrode, causing an ohmic-like insulator property in the SiO_2.[21] Hence, the voltage bias and power could effectively be applied to the FeO_x-transition layer and further reduce the operation voltages and variations. Of note, in Fig. 4c, the RTA-60 sec sample has the largest LRS/HRS current ratio because of the lowest HRS current. It is indicated that after the thermal treatment at 600°C for 60 sec, the trade-off between the diffusion effect of Fe atoms and the thickness of FeO_x-transition layer can be optimized.

An electroforming process was required for all the samples before repeating switching measurements. The forming voltage decreases markedly when the annealing time increases. After a 600°C annealing for 60 sec, the forming electric field of the as-deposited sample was reduced from 5.74 MV/cm to 0.13 MV/cm and further to 0.08 MV/cm when the annealing time increased to 30 min, resulting in a nearly formless requirement. It could be associated with an extensive Fe diffusion into the SiO_2 layer, which acted as impurities for the insulator and caused the soft-breakdown electric field to drop.[21]

For detailed analysis the devices' resistive witching behaviors and their electrical characteristics, Fig. 5 shows the statistical comparisons of set and reset electrical parameters for the different thermal treatment conditions. For the set process region, not only the mean value of V_{set} but also the variance of V_{set} becomes smaller with longer annealing time. Also, the set current increases and the set power maintains nearly constant while the annealing time increases except for the RTA-60 sec sample. Based on the recently studies, the set power at the initial current change point can be regarded as the beginning of chemical reduction reaction, which means that the resistance state is beginning to transfer from HRS to LRS.[22,23] Therefore, the same transformation energy of redox reaction from Fe_2O_3 phase to Fe_3O_4 phase in the FeO_x-transition layer can be predicted for all the samples, and the applied set power should be approximate constant when we exclude the power consumption within the ohmic-like SiO_x layer. On the other hand, for the reset process, it is also observed that both the mean value of V_{reset} and its variance become smaller with longer annealing time. However, the reset current remains constant in spite of the annealing treatments, and the reset power decreases with the increase of annealing time. According to the results of constant reset current, the reset process of the device is regarded as the chemical oxidation reaction with a necessary of sufficient Joule heat energy by localized current flow,[24,25] which would help the chemical redox reaction activate and transfer the chemical states from Fe_3O_4 phase to Fe_2O_3 phase. However, for the reset power decrease with the increase of the thermal annealing time, that is dominated by the reset voltage due the severe Fe diffusion effect, which results in ohmic-like insulator

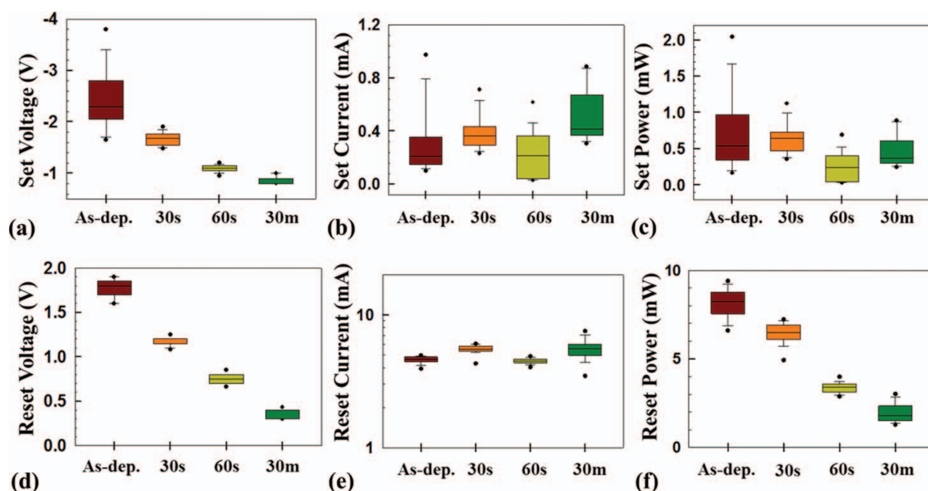

Figure 5. Statistical comparisons of set/reset voltage, set/reset current and set/reset power without (as-deposited condition) and with a thermal treatment of RTA-30 sec, RTA-60 sec and FA-30 min at 600°C samples.

Downloaded on 2014-04-28 to IP 140.113.38.11 address. Redistribution subject to ECS terms of use (see ecsdl.org/site/terms_use) unless CC License in place (see abstract).

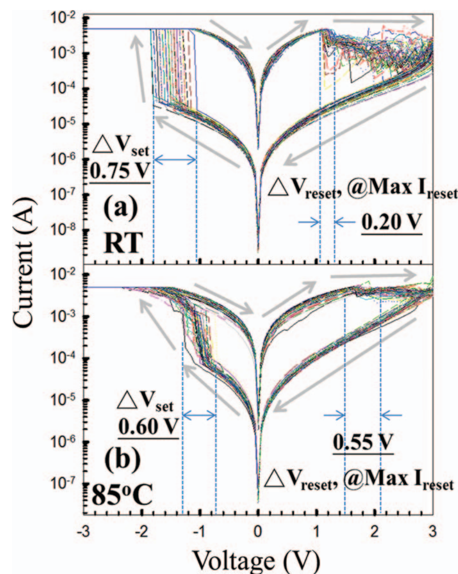

Figure 6. 50-cycle bipolar switching behaviors of the RTA-60 sec at (a) room temperature (RT) and (b) 85°C. The arrows indicate the voltage sweeping directions and variations of set and reset voltage value.

property in the SiO_2 layer. Hence, the voltage bias and power could effectively be applied to the FeO_x-transition layer and further reduce the variation of the electrical operation.[21]

Resistance switching behavior in high temperature environment.— The effect of measurement temperature during the repeating switching measurements at the same device is shown in the Figure 6a and 6b. Fig. 6a and 6b show the *I-V* electrical resistive switching behaviors of the RTA-60 sec samples for 50 cycles of switching at room temperature (RT) and at 85°C, respectively. The driving voltage was fixed at +/−3V on the bottom electrode while the top electrode was ground. The compliance current was fixed at 5 mA in the set process. There are several distinct differences: (1) For the set process, the switching current in the RT measurement is changed much more dramatically than at 85°C measurement. The set voltage for 85°C measurement condition as well as its variation is reduced, and its corresponding HRS current is increased compared to the RT testing condition. (2) For the reset process, the resistive switching behaviors at 85°C are gradually changed the transition current rather than drastically dropped at RT. Similarly, the statistic electrical parameters, such as LRS/HRS current and set/reset power, are also extracted to investigate and compare in detail between measurements at RT and 85°C, as shown in the Figure 7a and 7b, respectively. In Fig. 7a, the HRS current at 85°C is higher than at RT; meanwhile, the LRS current has the opposite trend, lower at 85°C. These results are consistent with our previous analyzes, which indicate that the HRS current

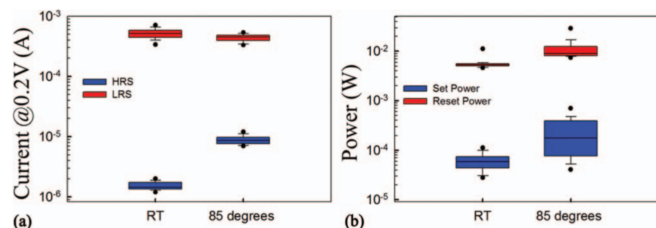

Figure 7. Statistical comparisons of (a) HRS/LRS current (b) set/reset power between the room temperature (RT) and 85°C in the $TiN/SiO_2/FeO_x/Fe/Pt$ structure with a thermal treatment of RTA-60 sec.

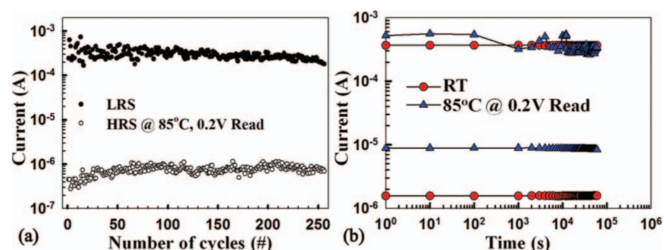

Figure 8. Reliability of (a) endurance test at 85°C and (b) retention test at room-temperature (RT) and 85°C for $TiN/SiO_2/FeO_x/Fe/Pt$ structures with a thermal treatment of RTA-60 sec.

transport behavior is dominated by the Poole–Frenkel emission, the current increases with the temperature, and the LRS current transport behavior follows the metal-type Ohm's law, the current decreases with the temperature increasing.[13] Most importantly, in Fig. 7b, the mean value of set and reset power as well as its variation increase in the 85°C measurements compared to in RT measurements. The possible explanation is that: for the reset process at high temperature, thermal fluctuations and chemical reaction activities would be much higher than at RT, even the compliance current limitation is clamped at fixed value during the set process. In other words, at 85°C, the chemical reduction activities during the set process would be much higher than at RT, which means that the FeO_x-transition layer at 85°C would be transformed more phases from Fe_2O_3 to Fe_3O_4 during the set process. Therefore, the formed conductive path would be much stronger and wider, to require higher or "overshooting" reset power to rupture the conductive filaments, as shown in Fig. 7b.[23] On the other hand, for the set process, as we mentioned previously, is the beginning of chemical reduction reaction, which means that the resistance state transfer from HRS to LRS at critical point. Therefore, for the set power characteristics, the parasitic power consumption at 85°C should be further considered due to the lower HRS resistance, which means that the applied set power could not be effectively supplied the transformation energy to the FeO_x-transition layer.[23] Although it seems contradictory with the thermodynamical process, the set power should reduce at high temperature, however, the effectively applied power for the FeO_x-transition layer should be considered, specifically in the high leaky device, a severe effect of divided power in the equivalent series circuit, causing the set power should be applied more at high temperature.

Finally, Figure 8a and 8b show the endurance reliability test at 85°C and retention performance for the RTA-60 sec sample at RT and 85°C, respectively. The readout of LRS and HRS is performed after applied −3 V / 3 V, and then, the current of LRSs or HRSs is recorded by a nondestructive process under 0.2 V reading voltage with a time interval. Under endurance reliability test at 85°C, the LRS and HRS of RTA-60 sec sample are able to bear at least 250 switching cycles and maintain two order resistance ratios without degradation, as shown in Fig. 8a. Also, for the retention reliability test at RT and 85°C, both of the measurement conditions are kept stable for more than 6×10^4 sec, and 10-years lifetime can be expected and confirm the nonvolatile nature of the device, as shown in Fig. 8b. However, under retention test at 85°C, it is observed that the data retention becomes unstable with a time interval, which indicates that a high chemical activity happens and further results in its chemical states of Fe_3O_4 and Fe_2O_3 exchanging slightly at high temperature.

Conclusions

Thermal treatment effect and high temperature testing behaviors on reproducible resistance switching characteristics of a $TiN/SiO_2/FeO_x/Fe$ structure were investigated. The thermal annealing results demonstrate the improvements of the switching parameters, such as forming voltage, V_{set}, V_{reset}, ΔV_{set} and ΔV_{reset}. According to the XRD and XPS depth profiles analyzes, exhibition of better

Downloaded on 2014-04-28 to IP 140.113.38.11 address. Redistribution subject to ECS terms of use (see ecsdl.org/site/terms_use) unless CC License in place (see abstract).

crystallinity of the FeO_x-transition layer with a wider Fe-diffused region would provide an effective iron oxide phase transformation region for resistance switching, and also, further reduce the switching power consumption. For detailed comparison the electrical characteristics between RT and 85°C measurement environment, the results show that the temperature-sensitive FeO_x-based memristor would be strongly affected by the temperature-dependent chemical redox reaction, which indicated possible resistive switching characteristics and mechanism. Moreover, high temperature reliability tests show that the FeO_x-containing memristor could be a possible future nonvolatile memory application.

Acknowledgment

This work was performed at National Science Council Core Facilities Laboratory for Nano-Science and Nano-Technology in Kaohsiung-Pingtung area and was supported by the National Science Council of the Republic of China under Contract Nos. NSC 100-2120-M-110-003.

References

1. T. C. Chang, F. Y. Jian, S. C. Chen, and Yu-Ting Tsai, *Mater. Today*, **14**, P526 (2011).
2. I. G. Baek, M. S. Lee, S. Seo, M. J. Lee, D. H. Seo, D. S. Suh, J. C. Park, S. O. Park, H. S. Kim, I. K. Yoo, U. I. Chung, and J. T. Moon, *Tech. Dig. - Int. Electron Devices Meet*, 587 (2004).
3. M. N. Kozicki, M. Park, and M. Mitkova, *IEEE Trans. Nanotechnol.*, **4**, 331 (2005).
4. M. Kawasaki, A. Sawa, and Y. Tokura, *Int. Conf. Solid State Devices Mater.*, 286, (2006).
5. J. E. Ralph and J. M. Woodcock, *J. Non-Cryst. Solids*, **7**, 236 (1972).
6. R. Dong, D. S. Lee, W. F. Xiang, S. J. Oh, D. J. Seong, S. H. Heo, H. J. Choi, M. J. Kwon, S. N. Seo, M. B. Pyun, M. Hasan, and H. Hwang, *Appl. Phys. Lett.*, **90**, 042107 (2007).
7. X. Wu, P. Zhou, J. Li, L. Y. Chen, H. B. Lv, Y. Y. Lin, and T. A. Tang, *Appl. Phys. Lett.*, **90**, 183507 (2007).
8. D. S. Lee, D. J. Seong, H. J. Choi, I. Jo, R. Dong, W. Xiang, S. Oh, M. Pyun, S. O. Seo, S. Heo, M. Jo, D. K. Hwang, H. K. Park, M. Chang, M. Hasan, and H. Hwang, *Tech. Dig. - Int. Electron Devices Meet*, 346733 (2006).
9. S. Q. Liu, N. J. Wu, and A. Ignatiev, *Appl. Phys. Lett.*, **76**, 2749 (2000).
10. D. S. Lee, H. J. Choi, H. J. Sim, D. H. Choi, H. S. Hwang, M. J. Lee, S. A. Seo, and I. K. Yoo, *IEEE Electron Device Lett.*, **26**, 719 (2005).
11. H. Lv, M. Wang, H. Wan, Y. Song, W. Luo, P. Zhou, T. Tang, Y. Lin, R. Huang, S. Song, J. G. Wu, H. M. Wu, and M. H. Chi, *Appl. Phys. Lett.*, **94**, 213502 (2009).
12. H. Lv and T. Tang, *IEEE Electron Device Lett.*, **31**, 1464 (2010).
13. L. W. Feng, C. Y. Chang, Y. F. Chang, W. R. Chen, S. Y. Wang, P. W. Chiang, and T. C. Chang, *Appl. Phys. Lett.*, **96**, 052111 (2010).
14. L. W. Feng, C. Y. Chang, Y. F. Chang, T. C. Chang, S. Y. Wang, S. C. Chen, C. C. Lin, S. C. Chen, and P. W. Chiang, *Appl. Phys. Lett.*, **96**, 222108 (2010).
15. S. B. Lee, S. C. Chae, S. H. Chang, and C. Liu, *Korean Appl. Phys.*, **51**, 96 (2007).
16. S. Muraoka, K. Osano, Y. Kanzawa, S. Mitani, S. Fujii, K. Katayama, Y. Katoh, Z. Wei, T. Mikawa, K. Arita, Y. Kawashima, R. Azuma, K. Kawai, K. Shimakawa, A. Odagawa, and T. Takagi, *Tech. Dig. - Int. Electron Devices Meet*, 227 (2007).
17. Y. F. Chang, L. W. Feng, and T. C. Chang, *Materials Chemistry and Physics*, **131**, 262 (2011).
18. Y. Ikeda, M. Takana, and Y. Bando, *Bull. Inst. Chem. Res., Kyoto Univ.*, **64**, 249 (1986).
19. H. Yanagihara, M. Hasegawa, E. Kita, Y. Wakabayashi, H. Sawa, and K. Siratori, *J. Phys. Soc. Jpn.*, **75**, 054708 (2006).
20. S. Kumari, C. Tripathi, A. P. Singh, D. Chauhan, R. Shrivastav, S. Dass, and V. R. Satsangi, *Curr. Sci.*, **91**, 1062 (2006).
21. T. W. Hickmott, *J. Appl. Phys.*, **100**, 083712 (2006).
22. C. Rohde, B. J. Choi, D. S. Jeong, S. Choi, J. S. Zhao, and C. S. Hwang, *Appl. Phys. Lett.*, **86**, 262907 (2005).
23. Y. F. Chang, T. C. Chang, and C. Y. Chang, *J. Appl. Phys.*, **110**, 053703 (2011).
24. A. Asamitsu, Y. Tomioka, H. Kuwahara, and Y. Tokura, *Nature (London)*, **388**, 50 (1997).
25. D. C. Kim, S. Seo, S. E. Ahn, D. S. Suh, M. J. Lee, B. H. Park, I. K. Yoo, I. G. Baek, H. J. Kim, E. K. Yim, J. E. Lee, S. O. Park, H. S. Kim, U-In Chung, J. T. Moon, and B. I. Ryu, *Appl. Phys. Lett.*, **88**, 202102 (2006).

Downloaded on 2014-04-28 to IP 140.113.38.11 address. Redistribution subject to ECS terms of use (see ecsdl.org/site/terms_use) unless CC License in place (see abstract).